https://doi.org/10.1016/j.optcom.2018.06.084

Hierarchically optical double-image correlation using 3D phase retrieval algorithm in fractional Fourier transform domain

Wen Chen[1,2,*]

[1]The Hong Kong Polytechnic University Shenzhen Research Institute, Shenzhen 518057, China
[2]Department of Electronic and Information Engineering, The Hong Kong Polytechnic University, Hong Kong, China
*Email: owen.chen@polyu.edu.hk

Abstract: In this paper, hierarchically optical double-image correlation is proposed by using 3D phase retrieval algorithm with a series of random function orders in fractional Fourier transform domain. At each hierarchical level, two grayscale input images are divided into particle-like points placed in 3D space, which are encoded into phase-only patterns using an iterative phase retrieval algorithm with a series of random function orders in fractional Fourier transform. The results illustrate that when the extracted phase-only patterns are compressed, optical double-grayscale-image correlation can be effectively conducted without the visualization of input information at each hierarchical level in 3D space. The proposed method provides a novel strategy for 3D optical security, and can effectively enhance the flexibility for the optically secured correlation in 3D space.

Keywords: Optical Correlation; 3D phase retrieval algorithm; Optical security.

1. Introduction

Phase retrieval[1–7] has been considered as one of the most important topics in optical imaging. Since only intensity patterns can be recorded, phase information should be extracted to determine the test sample parameters. In interference-based optical setup[8–13], phase-shifting and off-axis with spatial carrier are usually applied. In the coherent diffractive imaging or noninterferometric imaging[4–7,14,15], iterative operation between real and reciprocal spaces is usually designed and applied. Until now, there are a number of phase retrieval infrastructures and algorithms[1–15] which are applied in various fields, such as optical metrology, biomedical imaging and optical display.

In recent years, it is found that phase retrieval can also be applied as a promising method to generate phase-only patterns as ciphertext or key for optical security[16–19]. Original data or image can be encoded into one or several cascaded phase-only patterns by using phase retrieval algorithm, which is different from conventional double random phase encoding[20].

For instance, Gerchberg-Saxton algorithm[21] can be modified to encode the data or image into phase-only pattern. Since the generated phase-only patterns can be easily manufactured and applied nowsdays, it has attracted much attention in industrial sectors, such as logistics and biometric security. However, there are still some concerns in phase-retrieval-based optical security systems, such as convergence rate and security level. The researchers have been continuously developing novel infrastructures and algorithms to resolve the inherent problems in phase-retrieval-based optical security. For instance, Hwang et al.[22] modified conventional Gerchberg-Saxton algorithm to encode multiple inputs into phase-only patterns for capacity enhancement. Xiao et al.[23] proposed to modify Gerchberg-Saxton algorithm for multiple-image encoding with a cascaded structure. More recent developments about optical encryption and optical authentication can be found in Ref. [24].

However, it is concerned that previous work is limited to 2D processing, and to enhance system security 3D processing can be further introduced into phase-retrieval-based optical security system. Some related work[25–28] has been done. For instance, Chen et al.[25] have effectively designed particle-like points, and all points are placed in 3D space and further encoded into phase-only patterns. It has been illustrated that without knowledge of axial distances, the correct input cannot be extracted at any one section. Recently, this approach has been further studied for 3D Gerchberg-Saxton correlation[29], and it has been demonstrated that system security is dramatically enhanced without the visualization of input information in 3D space. However, the study in Ref. [29] used a relatively simple structure, and only single-image correlation has been investigated. It is desirable that more varied strategies can be developed to enhance the flexibility.

In this paper, optical double-image correlation is presented by using 3D phase retrieval algorithm with a hierarchical structure and a series of random function orders in fractional Fourier transform domain. At each hierarchical level, two grayscale input images are divided into particle-like points placed in 3D space, which are encoded into phase-only patterns using an iterative phase retrieval algorithm. It will be illustrated that when the extracted phase-only patterns are compressed, optical double-image correlation can be effectively and correctly conducted without the visualization of input information at each hierarchical level in 3D space.

2. Principles

Figures 1(a) and 1(b) show schematic setups for the proposed method at the 1st and 2nd hierarchical levels, respectively. Here, two grayscale input images are encoded at each hierarchical level, and for simplicity only two hierarchical levels are investigated. It can be straightforward to apply the proposed method with more hierarchical levels. Similarly to those in Refs. [25–27], each input image is divided into a series of particle-like points, and in this study 64×64 neighboring pixels are combined as a particle-like point as shown in Fig. 1. The 64 particle-like points are generated for each grayscale input image, and the generated particle-like points are placed at different axial positions.

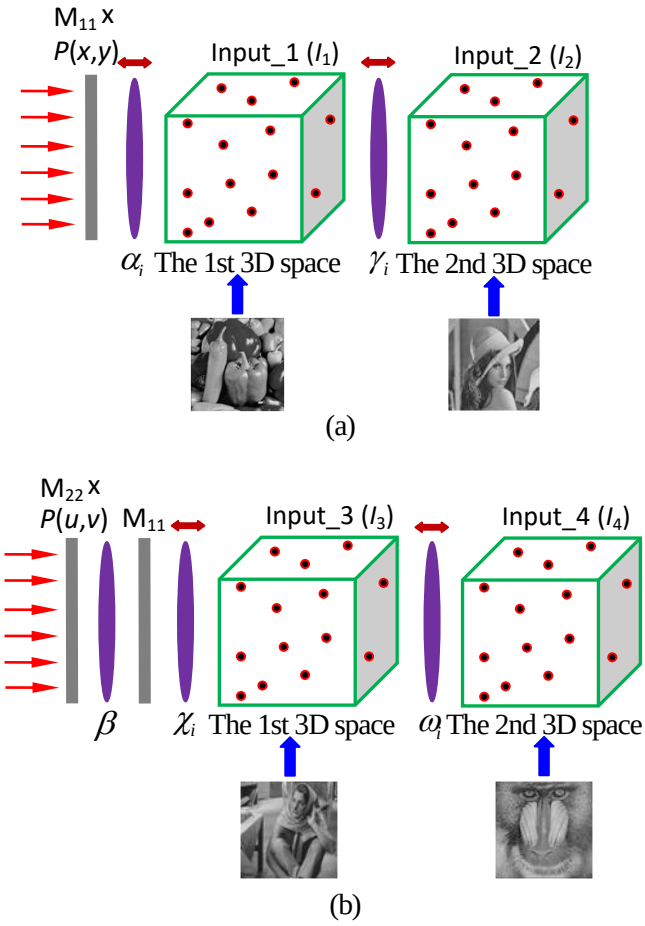

Fig. 1. (a) A schematic setup for the proposed 3D optical correlation method at the 1st hierarchical level, and (b) a schematic setup for the proposed 3D optical correlation method at the 2nd hierarchical level: M, phase-only mask; $\alpha,\beta,\gamma,\chi,\omega$, function orders in fractional Fourier transform. The lens can be axially translated to generate each function order in fractional Fourier transform. Integer i is 1, 2, 3,….,K. The input images can be found in http://sipi.usc.edu/database.

At the 1st hierarchical level, the objective is to encode all particle-like points (corresponding to the input images 1 and 2) into one phase-only pattern. The generated particle-like points are sequentially processed, and at the 1st hierarchical level a random phase-only map is first assumed to $M_1^{(i,n)}(x,y)$. Here, i denotes an index for each particle-like point (i.e., i=1,2,3,……,K), and n denotes the iteration number (i.e., n=1,2,3,……). The process between the phase-only pattern plane and the 1st 3D space can be described by

$$O(\xi_1^{(i)},\eta_1^{(i)}) = \mathrm{FrFT}_{\alpha_i}\left[M_1^{(i,n)}(x,y)\right], \tag{1}$$

where α_i denotes a series of random function orders in fractional Fourier transform between the phase-only pattern plane and the 1st 3D space, (x,y) denotes the coordinate for phase-

only pattern, (ξ_1,η_1) denotes the coordinate for transverse plane in the 1st 3D space, and FrFT denotes fractional Fourier transform described by[30,31]

$$\mathrm{FrFT}_\alpha\left[M_1(x)\right]=\int_{-\infty}^{+\infty}M_1(x)\rho_\alpha(\xi_1,x)\,dx, \tag{2}$$

where $\rho_\alpha(\xi_1,x)=\begin{cases}\Re\exp\left\{j\pi\left[\xi_1^2\cot\left(\alpha\pi/2\right)+x^2\cot\left(\alpha\pi/2\right)\right.\right. & \\ \left.\left.-2\xi_1 x\csc\left(\alpha\pi/2\right)\right]\right\} & \text{if } \alpha\neq 2m \\ \delta(\xi_1-x) & \text{if } \alpha=4m \\ \delta(\xi_1+x) & \text{if } \alpha=4m\pm 2\end{cases}$, m denotes an integer, $j=\sqrt{-1}$, and $\Re=\sqrt{1-j\cot\left(\alpha\pi/2\right)}$. The description of 2D FrFT is straightforward.

Subsequently, the complex-valued wavefront is updated by using the given information related to the 1st input image, and the updating process can be described by[25–27, 29]

$$\hat{O}(\xi_1^{(i)},\eta_1^{(i)})=\begin{cases}\left[2\Omega I_1(\xi_1,\eta_1)-\left|O(\xi_1^{(i)},\eta_1^{(i)})\right|\right]\dfrac{O(\xi_1^{(i)},\eta_1^{(i)})}{\left|O(\xi_1^{(i)},\eta_1^{(i)})\right|} & \\ \qquad\qquad if\ \ (\xi_1,\eta_1)\in i\,, & \\ O(\xi_1^{(i)},\eta_1^{(i)}) & \\ \qquad\qquad if\ \ (\xi_1,\eta_1)\notin i & \end{cases} \tag{3}$$

where $I_1(\xi_1,\eta_1)$ is the 1st grayscale input image, $|\ |$ denotes the modulus operation, $\hat{O}(\xi_1^{(i)},\eta_1^{(i)})$ denotes the updated complex-valued wavefront in the 1st 3D space, and Ω denotes a ratio between the summation of calculated output and the summation of the desired grayscale input image within the particle-like point i[25–27, 29].

Double-image encoding at each hierarchical level is studied here, and propagation process between the 1st 3D space and 2nd 3D space is further conducted as follows:

$$O(\xi_2^{(i)},\eta_2^{(i)})=\mathrm{FrFT}_{\gamma_i}\left[\hat{O}(\xi_1^{(i)},\eta_1^{(i)})\right], \tag{4}$$

where γ_i denotes a series of random function orders in fractional Fourier transform between the 1st 3D space and the 2nd 3D space, and (ξ_2,η_2) denotes the coordinate for transverse plane in the 2nd 3D space. Similarly to that in Eq. (3), the generated complex-valued wavefront is further updated by using a constraint of the 2nd grayscale input image, and the updating operation can be described by[25–27, 29]

$$\hat{O}(\xi_2^{(i)},\eta_2^{(i)})=\begin{cases}\left[2\Omega I_2(\xi_2,\eta_2)-\left|O(\xi_2^{(i)},\eta_2^{(i)})\right|\right]\dfrac{O(\xi_2^{(i)},\eta_2^{(i)})}{\left|O(\xi_2^{(i)},\eta_2^{(i)})\right|} & \\ \qquad\qquad if\ \ (\xi_2,\eta_2)\in i\,, & \\ O(\xi_2^{(i)},\eta_2^{(i)}) & \\ \qquad\qquad if\ \ (\xi_2,\eta_2)\notin i & \end{cases} \tag{5}$$

where $I_2(\xi_2,\eta_2)$ is the 2nd grayscale input image, and $\hat{O}(\xi_2^{(i)},\eta_2^{(i)})$ denotes the updated wavefront in the 2nd 3D space. It is worth noting that each time the symbol *i* simultaneously represents two particle-like points along the same longitudinal axis.

After the updated complex-valued wavefront is generated in the 2nd 3D space, back propagation is conducted to extract complex-valued wavefront in the phase-only pattern plane and an updated phase-only pattern can be obtained. This process is described by

$$\hat{M}_1^{(i,n)}(x,y)=\frac{\mathrm{FrFT}_{-(\alpha_i+\gamma_i)}\left[\hat{O}(\xi_2^{(i)},\eta_2^{(i)})\right]}{\left|\mathrm{FrFT}_{-(\alpha_i+\gamma_i)}\left[\hat{O}(\xi_2^{(i)},\eta_2^{(i)})\right]\right|}, \tag{6}$$

where $\hat{M}_1^{(i,n)}(x,y)$ is the updated phase-only pattern, and $\mathrm{FrFT}_{-(\alpha_i+\gamma_i)}$ denotes inverse fractional Fourier transform[30,31]. Equations (1)–(6) are sequentially implemented for all particle-like points until $i=K$. After all particle-like points are processed, one iterative operation is completed. Here, the error (difference)[29] between amplitude maps of two neighboring 2D wavefronts (using an incorporation of all decoded particle-like points) in the 2nd 3D space is calculated to judge whether the iterative operation can be stopped, and the difference (or error) is calculated by

$$\mathrm{Error}=\frac{\sum_{(\xi_2,\eta_2)}\left[\left|O_a^{(n)}(\xi_2,\eta_2)\right|-\left|O_a^{(n-1)}(\xi_2,\eta_2)\right|\right]^2}{512\times 512}, \tag{7}$$

where $O_a^{(n)}(\xi_2,\eta_2)$ denotes complex-valued wavefront obtained by incorporating all decoded particle-like points in the 2nd 3D space. After the threshold is satisfied, the finally updated phase-only pattern is considered as M1, i.e., $M_1(x,y)$. If the threshold is not satisfied, the updated phase-only pattern $\hat{M}_1^{(i,n)}(x,y)$ obtained in Eq. (6) is used for the next iteration, i.e., $n=n+1$.

To conduct optical correlation without observation of original input information, the extracted phase-only pattern $M_1(x,y)$ is further compressed, and only 15.0% pixels are randomly selected and maintained (other pixels are set as zero). The compressed phase-only pattern is denoted as $M_{1s}(x,y)$. Here, a random phase-only pattern $MH(x,y)$ is pre-generated, and the values are randomly distributed in a range of $[0,2\pi]$. Non-zero pixels in the phase-only pattern $M_{1s}(x,y)$ replace the corresponding pixels in phase-only pattern $MH(x,y)$ to generate a final phase-only pattern $M_{11}(x,y)$. It means that the maintained pixels of the originally extracted phase-only pattern $M_1(x,y)$ are embedded in the randomly-distributed phase-only pattern $M_{11}(x,y)$. For the decoding at the 1st hierarchical level, the key for the hidden pixel positions should be applied, and this complementary key is denoted as $P(x,y)$, i.e., a binary map.

At the 2nd hierarchical level [see Fig. 1(b)], phase-only pattern $M_{11}(x,y)$ obtained at the 1st hierarchical level is fixed in the optical path, and the objective is to encode two grayscale input images 3 and 4 into phase-only pattern M2. In Fig. 1(b), the process between the M2 plane and the 1st 3D space can be described by

$$O(\xi_1^{(i)},\eta_1^{(i)})=\mathrm{FrFT}_{\chi_i}\left(\left\{\mathrm{FrFT}_{\beta}\left[M_2^{(i,n)}(\mu,\nu)\right]\right\}M_{11}(x,y)\right), \tag{8}$$

where β denotes a FrFT function order between the M2 plane and the M11 plane, χ_i denotes a series of random function orders in fractional Fourier transform between the M11 plane and the 1st 3D space, and (μ,ν) denotes the coordinate for phase-only pattern M2.

Subsequently, the complex-valued wavefront is updated by using the given information related to the 3rd input image, and the updating process can be described by[25–27, 29]

$$\hat{O}(\xi_1^{(i)},\eta_1^{(i)})=\begin{cases}\left[2\Omega I_3(\xi_1,\eta_1)-\left|O(\xi_1^{(i)},\eta_1^{(i)})\right|\right]\dfrac{O(\xi_1^{(i)},\eta_1^{(i)})}{\left|O(\xi_1^{(i)},\eta_1^{(i)})\right|} & if\ (\xi_1,\eta_1)\in i,\\ O(\xi_1^{(i)},\eta_1^{(i)}) & if\ (\xi_1,\eta_1)\notin i\end{cases} \tag{9}$$

where $I_3(\xi_1,\eta_1)$ is the 3rd grayscale input image, and $\hat{O}(\xi_1^{(i)},\eta_1^{(i)})$ denotes the updated complex-valued wavefront in the 1st 3D space.

The propagation process between the 1st 3D space and 2nd 3D space is further conducted.

$$O(\xi_2^{(i)},\eta_2^{(i)})=\mathrm{FrFT}_{\omega_i}\left[\hat{O}(\xi_1^{(i)},\eta_1^{(i)})\right], \tag{10}$$

where ω_i denotes a series of random function orders in fractional Fourier transform between the 1st 3D space and the 2nd 3D space. The generated complex-valued wavefront is updated by using a constraint of the 4th grayscale input image, and the process can be described by[25–27, 29]

$$\hat{O}(\xi_2^{(i)},\eta_2^{(i)})=\begin{cases}\left[2\Omega I_4(\xi_2,\eta_2)-\left|O(\xi_2^{(i)},\eta_2^{(i)})\right|\right]\dfrac{O(\xi_2^{(i)},\eta_2^{(i)})}{\left|O(\xi_2^{(i)},\eta_2^{(i)})\right|} & if\ (\xi_2,\eta_2)\in i,\\ O(\xi_2^{(i)},\eta_2^{(i)}) & if\ (\xi_2,\eta_2)\notin i\end{cases} \tag{11}$$

where $I_4(\xi_2,\eta_2)$ is the 4th grayscale input image. It is worth noting that at the 2nd hierarchical level each time the symbol *i* simultaneously represents two particle-like points along the same longitudinal axis.

After the updated complex-valued wavefront is generated in the 2nd 3D space, back propagation is conducted to extract the complex-valued wavefront in the M2 plane and an updated phase-only pattern can be obtained. The process is described by

$$\hat{M}_2^{(i,n)}(\mu,\nu)=\frac{\mathrm{FrFT}_{-\beta}\left(\left\{\mathrm{FrFT}_{-(\chi_i+\omega_i)}\left[\hat{O}(\xi_2^{(i)},\eta_2^{(i)})\right]\right\}\left[M_{11}(x,y)\right]^*\right)}{\left|\mathrm{FrFT}_{-\beta}\left(\left\{\mathrm{FrFT}_{-(\chi_i+\omega_i)}\left[\hat{O}(\xi_2^{(i)},\eta_2^{(i)})\right]\right\}\left[M_{11}(x,y)\right]^*\right)\right|}, \tag{12}$$

where $\hat{M}_2^{(i,n)}(\mu,\nu)$ is the updated phase-only pattern, $\mathrm{FrFT}_{-(\chi_i+\omega_i)}$ and $\mathrm{FrFT}_{-\beta}$ denote inverse fractional Fourier transform[30,31], and asterisk denotes complex conjugate. Equations (8)–(12) are sequentially implemented for all particle-like points until *i*=*K*. After all particle-like points are processed, one iterative operation is completed. Here, the error (difference) is also calculated by using Eq. (7) in the 2nd 3D space to judge whether the iterative operation can be stopped. After the threshold is satisfied, the finally updated phase-only pattern is considered as M2, i.e., $M_2(\mu,\nu)$. To conduct optical correlation without observation of input

information, the extracted phase-only pattern M2 is further compressed, and only 13.0% pixels are randomly selected and maintained (other pixels are set as zero). Here, the compressed phase-only pattern is denoted as $M_{2s}(\mu,\nu)$. One new phase-only pattern $MH(\mu,\nu)$ is pre-generated, and the values are randomly distributed in a range of $[0,2\pi]$. Non-zero pixels in the phase-only pattern $M_{2s}(\mu,\nu)$ replace the corresponding pixels in phase-only pattern $MH(\mu,\nu)$ to generate a final phase-only pattern $M_{22}(\mu,\nu)$. Hence, a new binary map $P(\mu,\nu)$ is generated as a complementary security key. To show the encoding process at the 2nd hierarchical level, a flow chart is given in Fig. 2. In the proposed optical system, the finally generated phase-only patterns $M_{11}(x,y)$ and $M_{22}(\mu,\nu)$ are transmitted as ciphertexts to the authorized receiver. The binary maps and FrFT function orders $(\alpha,\beta,\gamma,\chi,\omega)$ are used as security keys.

During optical decoding, the generated phase-only pattern can be embedded into phase-only spatial light modulator, and the plane wave is generated for the illumination. At the 1st hierarchical level, the two input images can be decoded respectively by

$$\hat{I}_1(\xi_1,\eta_1)=\underset{(\xi_1,\eta_1)}{\Im}\left\{\underset{(\xi_1,\eta_1)}{\Re}\left|\mathrm{FrFT}_{\alpha_i}\left[M_{11}(x,y)P(x,y)\right]\right|^2\right\}, \tag{13}$$

$$\hat{I}_2(\xi_2,\eta_2)=\underset{(\xi_2,\eta_2)}{\Im}\left\{\underset{(\xi_2,\eta_2)}{\Re}\left|\mathrm{FrFT}_{\alpha_i+\gamma_i}\left[M_{11}(x,y)P(x,y)\right]\right|^2\right\}, \tag{14}$$

where $\Re$ is the selection operation in transverse domain, $\hat{I}_1(\xi_1,\eta_1)$ and $\hat{I}_2(\xi_2,\eta_2)$ denote the images respectively decoded in the 1st and 2nd 3D space at the 1st hierarchical level, and $\Im$ is the incorporation operation in transverse domain. At the 2nd hierarchical level, the two input images can be decoded respectively by

$$\hat{I}_3(\xi_1,\eta_1)=\underset{(\xi_1,\eta_1)}{\Im}\left[\underset{(\xi_1,\eta_1)}{\Re}\left|\mathrm{FrFT}_{\chi_i}\left(\left\{\mathrm{FrFT}_{\beta}\left[M_{22}(\mu,\nu)P(\mu,\nu)\right]\right\}M_{11}(x,y)\right)\right|^2\right], \tag{15}$$

$$\hat{I}_4(\xi_2,\eta_2)=\underset{(\xi_2,\eta_2)}{\Im}\left[\underset{(\xi_2,\eta_2)}{\Re}\left|\mathrm{FrFT}_{\chi_i+\omega_i}\left(\left\{\mathrm{FrFT}_{\beta}\left[M_{22}(\mu,\nu)P(\mu,\nu)\right]\right\}M_{11}(x,y)\right)\right|^2\right], \tag{16}$$

where $\hat{I}_3(\xi_1,\eta_1)$ and $\hat{I}_4(\xi_2,\eta_2)$ denote the decoded images obtained in the 1st and 2nd 3D space at the 2nd hierarchical level, respectively.

Since the decoded images are noisy without the visualization of input information due to the designed optical system in this study, they can be respectively correlated with the original input images stored in a separated database for the verification. Even the authorized receivers cannot view original input images, and only an interface can be given to conduct the verification operation. The nonlinear correlation algorithm[29,32–40] is applied here, and the generalized form is described by[29,32–40]

$$D(\xi,\eta)=\left|\mathrm{IFT}\left(\left|\left\{\mathrm{FT}\left[I(\xi,\eta)\right]\right\}\left\{\mathrm{FT}\left[\hat{I}(\xi,\eta)\right]\right\}^*\right|^{t-1}\left\{\mathrm{FT}\left[I(\xi,\eta)\right]\right\}\left\{\mathrm{FT}\left[\hat{I}(\xi,\eta)\right]\right\}^*\right)\right|^2, \tag{17}$$

where $D(\xi,\eta)$ is the generated nonlinear correlation distribution[29,32–40], and FT and IFT denote Fourier transform and inverse Fourier transform, respectively. Here, strength of the applied nonlinearity (i.e., t) is set as 0.30[29,32–40]. To show optical decoding and optical correlation process at the 2nd hierarchical level, a flow chart is given in Fig. 3.

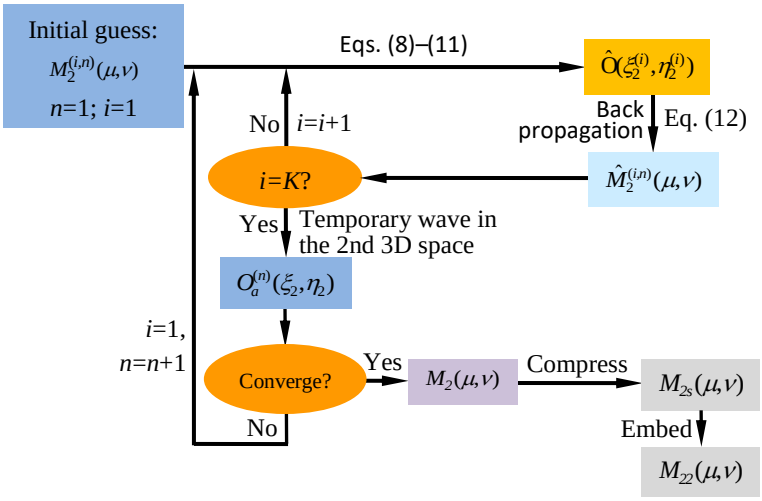

Fig. 2. Flow chart for the 3D optical encoding process at the 2nd hierarchical level. For the sake of brevity, flow chart at the 1st hierarchical level is not given here.

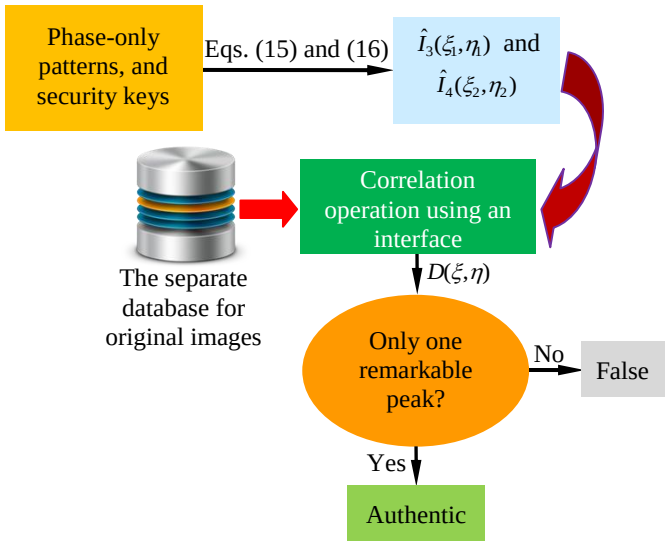

Fig. 3. Flow chart for optical decoding and optical correlation process at the 2nd hierarchical level. For the sake of brevity, flow chart at the 1st hierarchical level is not given here.

3. Results and discussion

The setups in Figs. 1(a) and 1(b) are computationally conducted for illustrating feasibility and effectiveness of the proposed 3D hierarchically optical correlation system. A collimated plane wave is generated in the optical path, such as by using a pinhole and a lens, and the laser wavelength is 632.8 nm. At each hierarchical level, two grayscale input images are encoded, and 64×64 neighboring pixels of each input image are combined as a particle-like point as shown in Figs. 1(a) and 1(b). Hence, 64 particle-like points are generated for each grayscale input image. Here, a series of random function orders in fractional Fourier transform are applied. The FrFT function order β is 0.55, and $\alpha,\gamma,\chi,\omega$ are randomly distributed in a range of [0.20, 0.70], [0.15, 0.85], [0.30, 0.90] and [0.25, 0.95], respectively. For the sake of brevity, only two hierarchical levels are studied, and it could be straightforward to apply the proposed method with more hierarchical levels. At the 1st hierarchical level two grayscale (8 bits) input images of "Peppers" and "Lena" (http://sipi.usc.edu/database) are encoded, and at the 2nd hierarchical level two grayscale (8 bits) input images of "Barbara" and "Baboon" are encoded. In the proposed optical system, the encoding process is conducted by using the proposed 3D phase retrieval algorithm to find approximate solutions for a phase-only pattern at each hierarchical level under the given constraints, such as a series of random FrFT function orders and grayscale input image. A digital method is applied for the encoding, and both digital and optical approaches can be flexibly used for the decoding and correlation.

Figure 4(a) shows a relationship between the number of iterations and the calculated errors (logarithm scale) at the 1st hierarchical level during the encoding. It can be seen that only 20 iterations are requested. The extracted phase-only pattern $M_1(x,y)$ is shown in Fig. 4(b), and the compressed phase-only pattern $M_{1s}(x,y)$ is shown in Fig. 4(c). Only 15.0% pixels of that in Fig. 4(b) are maintained, and others are set as zero. It can be seen that the two grayscale input images are fully encoded, and only a noisy phase-only pattern is generated. One phase-only pattern $MH(x,y)$ is pre-generated as shown in Fig. 4(d), and the finally generated phase-only pattern $M_{11}(x,y)$ is shown in Fig. 4(e). It can be seen that it is difficult to visually observe the embedded information related to $M_{1s}(x,y)$ from $M_{11}(x,y)$. At the 1st hierarchical level, a binary map $P(x,y)$ is generated as a complementary security key for detecting the embedded pixels. Figure 4(f) shows the binary map $P(x,y)$, and one enlarged part is given in an inset to show the sparsity. At the 2nd hierarchical level, the phase-only pattern $M_{11}(x,y)$ is fixed in the optical path, and the encoding objective is to extract phase-only pattern $M_2(\mu,\nu)$. Figure 5(a) shows a relationship between the number of iterations and the calculated errors (logarithm scale) at the 2nd hierarchical level during the encoding. It is illustrated that a rapid convergence rate is achieved in the proposed 3D phase retrieval algorithm at the 2nd hierarchical level. Figure 5(b) shows the extracted phase-only pattern $M_2(\mu,\nu)$, and its compressed form $M_{2s}(\mu,\nu)$ is shown in Fig. 5(c). Here, only 13.0% pixels of that in Fig. 5(b) are maintained, and others are set as zero. One phase-only pattern $MH(\mu,\nu)$ is pre-generated as shown in Fig. 5(d), and the finally generated phase-only pattern $M_{22}(\mu,\nu)$ is

shown in Fig. 5(e). It can be seen that it is difficult to visually observe the embedded information related to $M_{2s}(\mu,\nu)$ from $M_{22}(\mu,\nu)$. At the 2nd hierarchical level, a binary map $P(\mu,\nu)$ is generated as a complementary security key. Figure 5(f) shows the binary map $P(\mu,\nu)$, and one enlarged part is further given in the inset to show the sparsity.

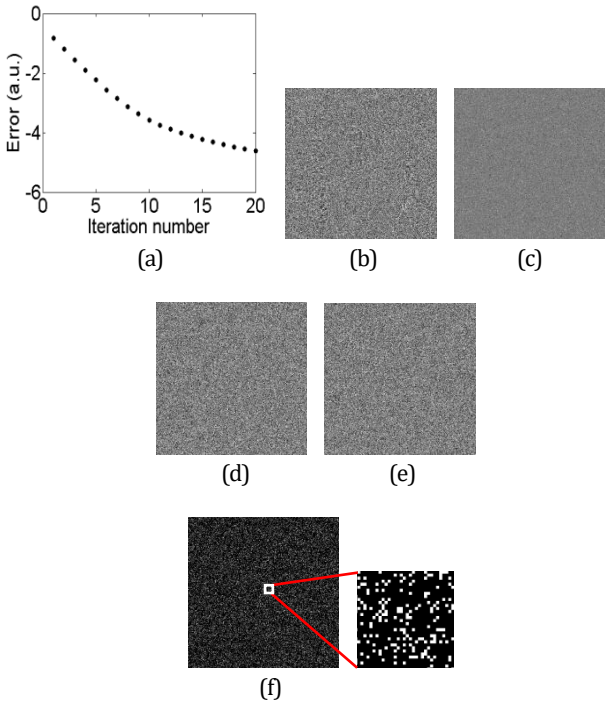

Fig. 4. The 1st hierarchical level: (a) a relationship between the number of iterations and the calculated errors (logarithm scale) obtained during the encoding, (b) the extracted phase-only pattern $M_1(x,y)$, (c) the compressed phase-only pattern $M_{1s}(x,y)$, (d) one random phase-only pattern $MH(x,y)$, (e) the finally generated phase-only pattern $M_{11}(x,y)$, and (f) a binary map $P(x,y)$. An enlarged part is given in the inset to show the sparsity.

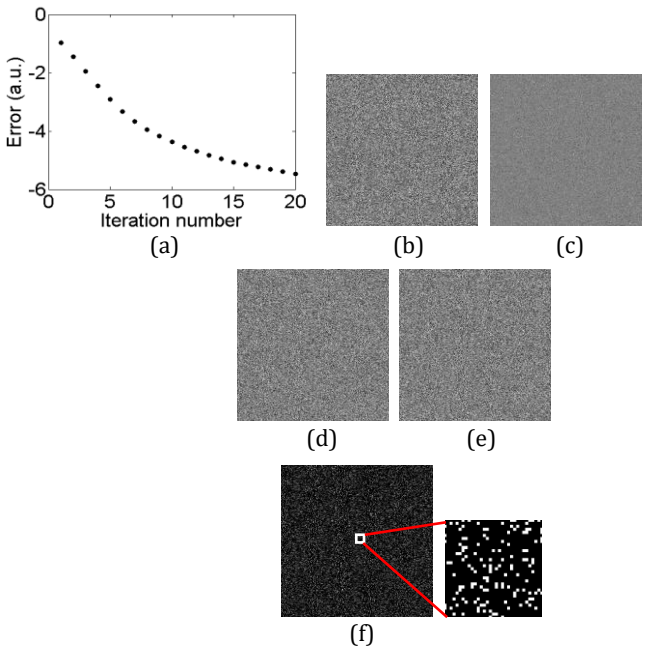

Fig. 5. The 2nd hierarchical level: (a) a relationship between the number of iterations and the calculated errors (logarithm scale) during the encoding, (b) the extracted phase-only pattern $M_2(\mu,\nu)$, and (c) the compressed form $M_{2s}(\mu,\nu)$, (d) a random phase-only pattern $MH(\mu,\nu)$, (e) the finally generated phase-only pattern $M_{22}(\mu,\nu)$, and (f) a binary map $P(\mu,\nu)$. An enlarged part is given in the inset to show the sparsity.

When the phase-only pattern and security keys are correctly applied (such as by authorized receiver) by using the setup in Fig. 1(a) at the 1st hierarchical level, the two input images are decoded as shown in Figs. 6(a) and 6(b), respectively. The correlation coefficient (CC) for Figs. 6(a) and 6(b) is 0.0778 and 0.0451, respectively. Due to the designed strategy, the decoded images cannot visually render the input information. Since these decoded images still contain sparsely but invisibly useful data, they can be correlated with the original input images stored in a separated database which is also not visible to the authorized receiver. Figures 6(c) and 6(d) show the generated nonlinear correlation maps corresponding to those in Figs. 6(a) and 6(b), respectively. It can be seen in Figs. 6(c) and 6(d) that only one remarkable peak is generated to confirm the identity of the receiver or the use of correct security keys. In practice, some parameters could be pre-defined for the standard nonlinear correlation distribution to judge whether the generated correlation map is accurate or not.

At the 2nd hierarchical level, when the phase-only patterns and security keys are correctly applied, the two input images are decoded as shown in Figs. 6(e) and 6(f). The CC values for Figs. 6(e) and 6(f) are 0.0464 and 0.0343, respectively. Figures 6(g) and 6(h) show the generated nonlinear correlation maps corresponding to those in Figs. 6(e) and 6(f), respectively. It is also illustrated that the decoded images obtained at the 2nd hierarchical

level can be correctly verified, and useful information hidden in the decoded images can be effectively correlated with the original input images for the verification.

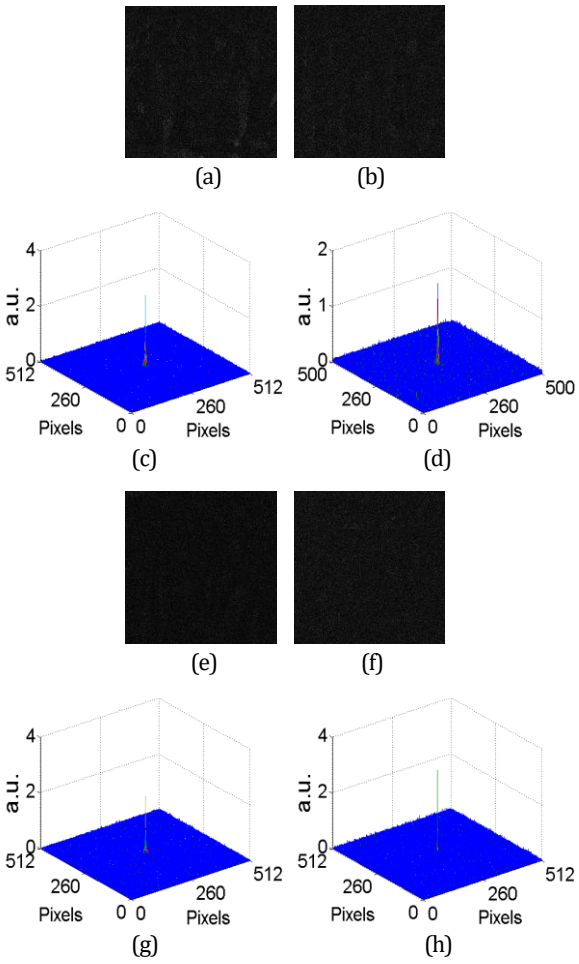

Fig. 6. (a) and (b) The decoded images obtained at the 1st hierarchical level when the phase-only pattern and security keys are correctly applied, and (c) and (d) the generated nonlinear correlation maps respectively corresponding to (a) and (b). (e) and (f) The decoded images obtained at the 2nd hierarchical level when the phase-only patterns and security keys are correctly applied, and (g) and (h) the generated nonlinear correlation maps respectively corresponding to (e) and (f).

Performance of the proposed 3D hierarchically optical correlation system is further analyzed. When phase-only pattern $M_{11}(x,y)$ is contaminated by noise (zero mean with variance of 0.06) at the 1st hierarchical level during the decoding, the two input images are decoded as shown in Figs. 7(a) and 7(b), respectively. The CC values for Figs. 7(a) and 7(b) are 0.0745 and 0.0430, respectively. Figures 7(c) and 7(d) show the generated nonlinear

correlation maps corresponding to those in Figs. 7(a) and 7(b), respectively. It can be seen in Figs. 7(c) and 7(d) that only one remarkable peak is still generated to confirm the identity of the receiver or the use of correct security keys. When 128×128 pixels of phase-only pattern $M_{11}(x,y)$ are occluded at the 1st hierarchical level during the decoding, the two input images are decoded as shown in Figs. 7(e) and 7(f), respectively. The CC values for Figs. 7(e) and 7(f) are 0.0767 and 0.0414, respectively. Figures 7(g) and 7(h) show the generated nonlinear correlation maps corresponding to those in Figs. 7(e) and 7(f), respectively. It can be seen in Figs. 7(g) and 7(h) that only one remarkable peak is generated, and the proposed method shows high robustness against the contaminations.

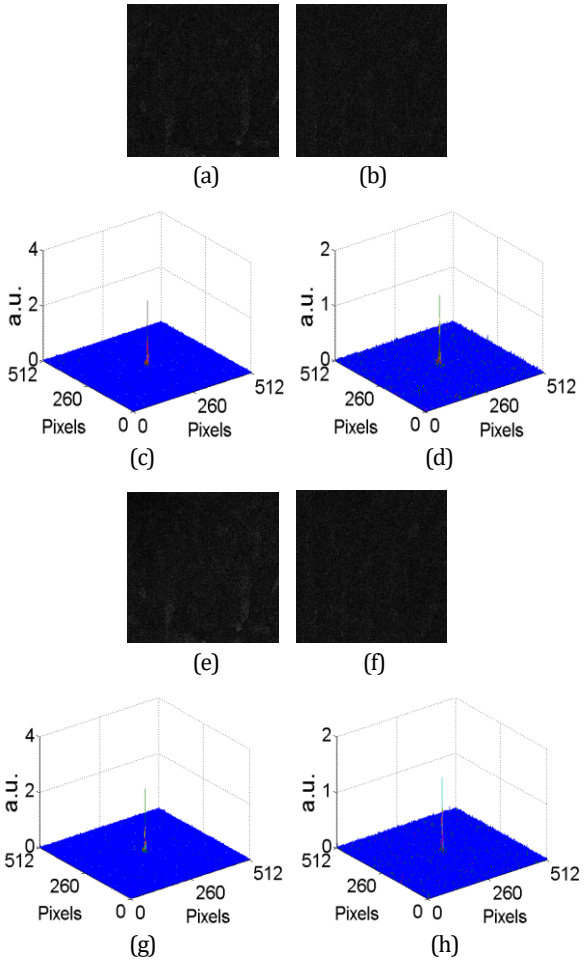

Fig. 7. The 1st hierarchical level: (a) and (b) two decoded images obtained when phase-only pattern $M_{11}(x,y)$ is contaminated by noise (zero mean with variance of 0.06) during the decoding, and (c) and (d) the generated nonlinear correlation maps respectively corresponding to that in (a) and (b). (e) and (f) Two decoded images obtained when 128×128 pixels of phase-only pattern $M_{11}(x,y)$ are occluded during the decoding, and (g) and (h) the generated nonlinear correlation maps respectively corresponding to that in (e) and (f).

Performance of security keys in the proposed optical system is also studied. When only random FrFT function orders α_i are incorrect at the 1st hierarchical level during the decoding, two input images are decoded as shown in Figs. 8(a) and 8(b), respectively. The CC values for Figs. 8(a) and 8(b) are 0.0165 and 0.0060, respectively. Figures 8(c) and 8(d) show the generated nonlinear correlation maps corresponding to that in Figs. 8(a) and 8(b), respectively. It can be seen in Figs. 8(c) and 8(d) that only noisy correlation distributions are generated, when security key is incorrectly used during the decoding. When only the series of random FrFT function orders γ_i is incorrect at the 1st hierarchical level during the decoding, the 1st input image can be correctly decoded and verified but the 2nd input image cannot. For the sake of brevity, analysis of random FrFT function orders γ_i is not presented here.

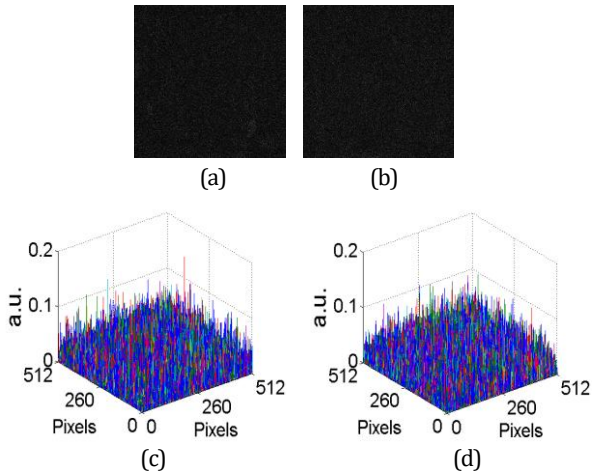

Fig. 8. The 1st hierarchical level: (a) and (b) two decoded images obtained when only FrFT function orders α_i are incorrect during the decoding, and (c) and (d) the generated nonlinear correlation maps respectively corresponding to that in (a) and (b).

Performance of the proposed 3D hierarchically optical correlation system is also analyzed at the 2nd hierarchical level. When phase-only pattern $M_{22}(\mu,\nu)$ is contaminated by noise (zero mean with variance of 0.06) at the 2nd hierarchical level during the decoding, the two input images are decoded as shown in Figs. 9(a) and 9(b), respectively. The CC values for Figs. 9(a) and 9(b) are 0.0438 and 0.0316, respectively. Figures 9(c) and 9(d) show the generated nonlinear correlation maps corresponding to those in Figs. 9(a) and 9(b), respectively. It can be seen in Figs. 9(c) and 9(d) that only one remarkable peak is generated to confirm the identity of the receiver or the use of correct security keys. When 128×128 pixels of phase-only pattern $M_{22}(\mu,\nu)$ are occluded at the 2nd hierarchical level during the decoding, two input images are decoded as shown in Figs. 9(e) and 9(f), respectively. The CC values for Figs. 9(e) and 9(f) are 0.0379 and 0.0284, respectively. Figures 9(g) and 9(h) show the generated

nonlinear correlation maps corresponding to those in Figs. 9(e) and 9(f), respectively. It can be seen in Figs. 9(g) and 9(h) that only one remarkable peak is also generated, and the proposed method shows high robustness against the contaminations. For the sake of brevity, analysis of security keys at the 2nd hierarchical level is not presented here.

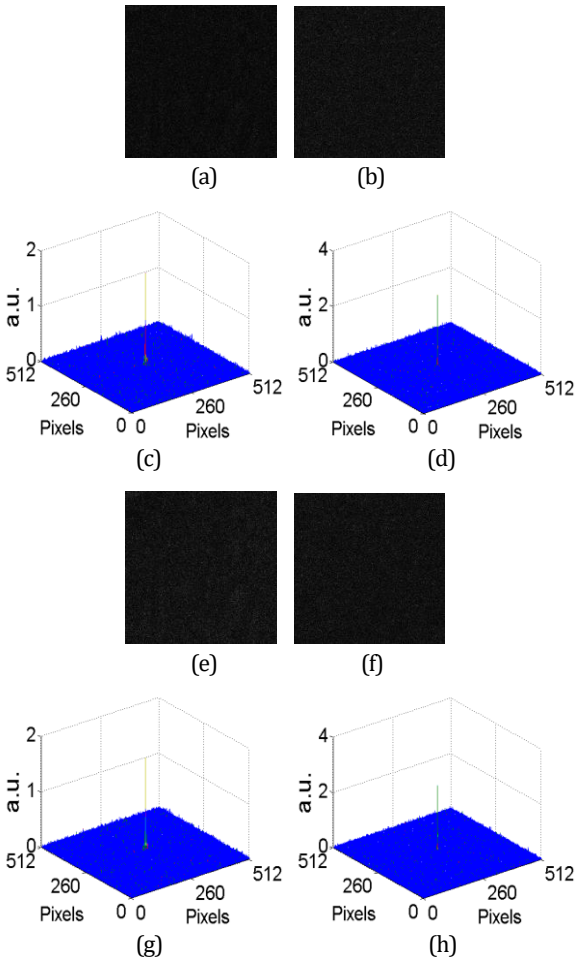

Fig. 9. The 2nd hierarchical level: (a) and (b) two decoded images obtained when phase-only pattern $M_{22}(\mu,\nu)$ is contaminated by noise (zero mean with variance of 0.06) during the decoding, and (c) and (d) the generated nonlinear correlation maps respectively corresponding to those in (a) and (b). (e) and (f) Two decoded images obtained when 128×128 pixels of phase-only pattern $M_{22}(\mu,\nu)$ are occluded during the decoding, and (g) and (h) the generated nonlinear correlation maps respectively corresponding to those in (e) and (f).

Discrimination capability of the proposed method is further investigated and analyzed. When another two grayscale input images ("Elaine" and "Goldhill" from http://sipi.usc.edu/database) are encoded by using the proposed method at the 2nd hierarchical level, these two new input images can be decoded as shown in Figs. 10(a) and 10(b) by using correct security keys. The CC values for Figs. 10(a) and 10(b) are 0.0358 and 0.0251, respectively. Here, all other setup parameters are the same as those used for Figs. 6(e) and 6(f). Figure 10(c) shows the generated nonlinear correlation map obtained between that in Fig. 10(a) and the original 3rd grayscale input image (i.e., "Barbara"), and Fig. 10(d) shows the generated nonlinear correlation map obtained between that in Fig. 10(b) and the original 4th grayscale input image (i.e., "Baboon"). As seen in Figs. 10(c) and 10(d), the proposed method shows high discrimination capability. Many other grayscale input images are also used for the discrimination capability test, and results similar to Figs. 10(c) and 10(d) are always generated. For the sake of brevity, discrimination capability of the proposed method is tested only at the 2nd hierarchical level.

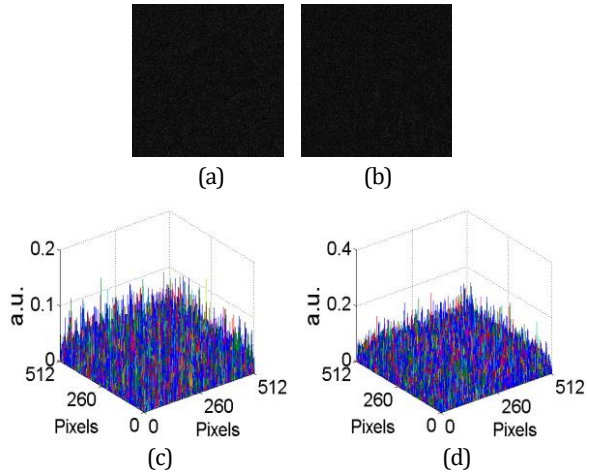

Fig. 10. Discrimination capability at the 2nd hierarchical level: (a) and (b) two decoded images obtained by using correct security keys when another two new grayscale input images are encoded by using the proposed method at the 2nd hierarchical level, (c) the generated nonlinear correlation map obtained between that in (a) and the original 3rd grayscale input image, and (d) the generated nonlinear correlation map obtained between that in (b) and the original 4th grayscale input image.

Since 3D hierarchically optical correlation is designed and applied in this study, any decoded image obtained at only one transverse section cannot provide sufficient information for correct verification at each hierarchical level. Figure 11(a) shows a decoded image obtained at the 1st hierarchical level, when only one FrFT function order of 0.30 is applied between the phase-only pattern plane and the 3D space. Figure 11(c) shows the generated

correlation distribution obtained between that in Fig. 11(a) and the original 1st grayscale input image (i.e., "Peppers"), and Fig. 11(d) shows the generated correlation distribution obtained between that in Fig. 11(a) and the original 2nd grayscale input image (i.e., "Lena"). Figure 11(b) shows a decoded image obtained at the 1st hierarchical level, when only one FrFT function order of 0.50 is applied between the phase-only pattern plane and the 3D space. Figure 11(e) shows the generated correlation distribution obtained between that in Fig. 11(b) and the original 1st grayscale input image, and Fig. 11(f) shows the generated correlation distribution obtained between that in Fig. 11(b) and the original 2nd grayscale input image. It can be seen in Figs. 11(c)–11(f) that only a noisy correlation map can be generated, when only one sectional decoding is conducted at the 1st hierarchical level. Similar phenomena can also be observed at the 2nd hierarchical level, and the results are shown in Figs. 12(a)–12(f).

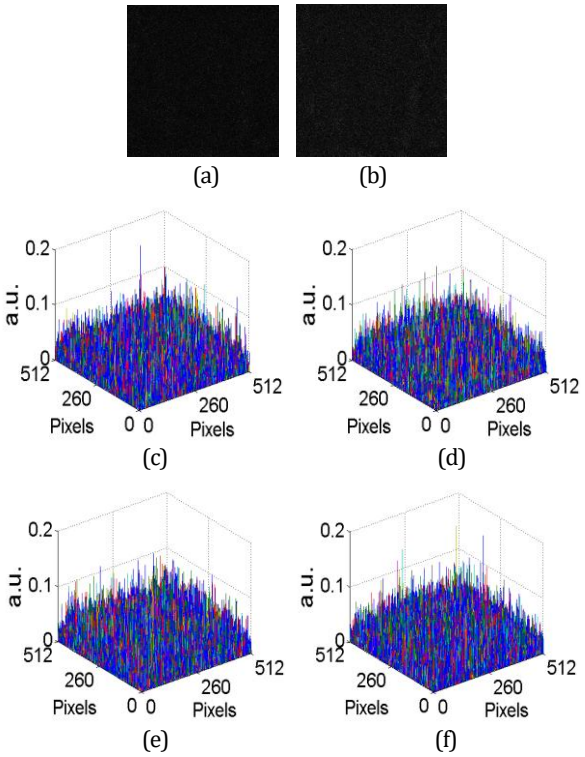

Fig. 11. A decoded image obtained at the 1st hierarchical level when only one FrFT function order of (a) 0.30 or (b) 0.50 is applied between the phase-only pattern plane and the 3D space, (c) the generated correlation distribution obtained between that in (a) and the original 1st grayscale input image (i.e., "Peppers"), (d) the generated correlation distribution obtained between that in (a) and the original 2nd grayscale input image (i.e., "Lena"), (e) the generated correlation distribution obtained between that in (b) and the original 1st grayscale input image, and (f) the generated correlation distribution obtained between that in (b) and the original 2nd grayscale input image.

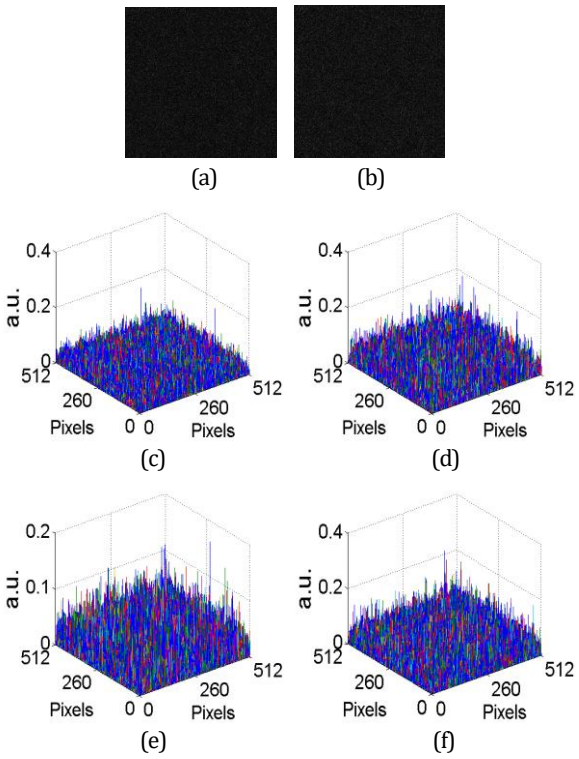

Fig. 12. A decoded image obtained at the 2nd hierarchical level when only one FrFT function order of (a) 0.30 or (b) 0.50 is applied between the phase-only pattern (M11) plane and the 3D space, (c) the generated correlation distribution obtained between that in (a) and the original 3rd grayscale input image (i.e., "Barbara"), (d) the generated correlation distribution obtained between that in (a) and the original 4th grayscale input image (i.e., "Baboon"), (e) the generated correlation distribution obtained between that in (b) and the original 3rd grayscale input image, and (f) the generated correlation distribution obtained between that in (b) and the original 4th grayscale input image.

Advantages of the proposed method and comparison to previous work are briefly described and discussed as follows: (1) Different from previous work[29], the proposed method has successfully decoded and verified more than one grayscale input image in 3D space at each hierarchical level. (2) The proposed method has effectively applied a series of random FrFT function orders in 3D optical correlation system, and they can be considered as significant security keys. (3) Hierarchical structure, for the first time, has been applied in phase-retrieval-based 3D optical correlation system, which provides much flexibility for the design. (4) Compared with the work in Refs. [19,25–27], the proposed method can achieve

the higher security, since hierarchically optical correlation without visualization of input information is conducted in 3D space.

4. Conclusions

The hierarchically optical double-image correlation has been presented by using 3D phase retrieval algorithm with a series of random function orders in fractional Fourier transform domain. At each hierarchical level, two input images are divided into particle-like points placed in 3D space, which are encoded into phase-only pattern using an iterative phase retrieval algorithm. The computational results illustrate that the optical double-grayscale-image correlation can be effectively conducted at each hierarchical level in 3D space, and high security is guaranteed at each hierarchical level in 3D space. The proposed method provides a novel strategy for 3D optical security, and can effectively enhance the flexibility for the optically secured correlation in 3D space.

Acknowledgements

This work was supported by the National Natural Science Foundation of China (NSFC) (61605165), Hong Kong Research Grants Council Early Career Scheme (25201416), Shenzhen Science and Technology Innovation Commission through Basic Research Program (JCYJ20160531184426473), and The Hong Kong Polytechnic University (4-BCDY, G-YBVU, 4-ZZHM and 1-ZE5F).

References

[1] M. R. Teague, "Deterministic phase retrieval: a Green's function solution," J. Opt. Soc. Am. **73**, 1434–1441 (1983).

[2] M. G. Raymer, M. Beck, and D. F. McAlister, "Complex wave-field reconstruction using phase-space tomography," Phys. Rev. Lett. **72**, 1137–1140 (1994).

[3] J. R. Fienup, "Phase retrieval algorithms: a comparison," Appl. Opt. **21**, 2758–2769 (1982).

[4] J. Zou, M., I. Vartanyants, M. Gao, R. Zhang, and L. A. Nagahara, "Atomic resolution imaging of a carbon nanotube from diffraction intensities," Science **300**, 1419–1421 (2003).

[5] J. Miao, D. Sayre, and H. N. Chapman, "Phase retrieval from the magnitude of the Fourier transforms of nonperiodic objects," J. Opt. Soc. Am. A **15**, 1662–1669 (1998).

[6] V. Elser, "Phase retrieval by iterated projections," J. Opt. Soc. Am. A **20**, 40–55 (2003).

[7] J. Miao, P. Charalambous, J. Kirz, and D. Sayre, "Extending the methodology of X-ray crystallography to allow imaging of micrometer-sized non-crystalline specimens," Nature **400**, 342–344 (1999).

[8] E. Cuche, P. Marquet, and C. Depeursinge, "Spatial filtering for zero-order and twin-image elimination in digital off-axis holography," Appl. Opt. **39**, 4070–4075 (2000).

[9] E. Cuche, F. Bevilacqua, and C. Depeursinge, "Digital holography for quantitative phase-contrast imaging," Opt. Lett. **24**, 291–293 (1999).

[10] T. Kreis, Handbook of Holographic Interferometry: Optical and Digital Methods (Wiley-VCH, Weinheim, 2005).

[11] K. Creath, “Phase-shifting speckle interferometry,” Appl. Opt. **24**, 3053–3058 (1985).
[12] I. Yamaguchi and T. Zhang, “Phase-shifting digital holography,” Opt. Lett. **22**, 1268–1270 (1997).
[13] M. Takeda, H. Ina, and S. Kobayashi, “Fourier-transform method of fringe-pattern analysis for computer-based topography and interferometry,” J. Opt. Soc. Am. **72**, 156–160 (1982).
[14] W. Chen and X. Chen, “Quantitative phase retrieval of a complex-valued object using variable function orders in the fractional Fourier domain,” Opt. Express **18**, 13536–13541 (2010).
[15] C. Wu, T. W. Ng, and A. Neild, “Phase and amplitude retrieval of objects embedded in a sinusoidal background from its diffraction pattern,” App. Opt. **49**, 1831–1837 (2010).
[16] R. K. Wang, I. A. Watson, and C. Chatwin, “Random phase encoding for optical security,” Opt. Eng. **35**, 2464–2469 (1996).
[17] W. Chen and X. Chen, “Optical multiple-image authentication based on modified Gerchberg-Saxton algorithm with random sampling,” Opt. Commun. **318**, 128–132 (2014).
[18] Z. Liu, L. Xu, C. Lin, and S. Liu, “Image encryption by encoding with a nonuniform optical beam in gyrator transform domains,” Appl. Opt. **49**, 5632–5637 (2010).
[19] W. Chen, X. Chen, A. Stern, and B. Javidi, “Phase-modulated optical system with sparse representation for information encoding and authentication,” IEEE Photon. J. **5**, 6900113 (2013).
[20] P. Refregier and B. Javidi, “Optical image encryption based on input plane and Fourier plane random encoding,” Opt. Lett. **20**, 767–769 (1995).
[21] R. W. Gerchberg and W. O. Saxton, “A practical algorithm for the determination of phase from image and diffraction plane pictures,” Optik (Stuttgart) **35**, 237–246 (1972).
[22] H. E. Hwang, H. T. Chang, and W. N. Lie, “Multiple-image encryption and multiplexing using a modified Gerchberg-Saxton algorithm and phase modulation in Fresnel-transform domain,” Opt. Lett. **34**, 3917–3919 (2009).
[23] Y. L. Xiao, X. Zhou, S. Yuan, Q. Liu, and Y. C. Li, “Multiple-image optical encryption: an improved encoding approach,” Appl. Opt. **48**, 2686–2692 (2009).
[24] Ayman Al Falou, Advanced secure optical image processing for communications (IOP Publishing Ltd, 2018).
[25] W. Chen, X. Chen, and Colin J. R. Sheppard, “Optical image encryption based on phase retrieval combined with three-dimensional particle-like distribution,” J. Opt. **14**, 075402 (2012).
[26] W. Chen and X. Chen, “Interference-based optical image encryption using three-dimensional phase retrieval,” Appl. Opt. **51**, 6076–6083 (2012).
[27] W. Chen, “Optical multiple-image encryption using three-dimensional space,” IEEE Photon. J. **8**, 6900608 (2016).
[28] M. Cho and B. Javidi, "Three-dimensional photon counting double-random-phase encryption," Opt. Lett. **38**, 3198–3201 (2013).
[29] W. Chen, “3D Gerchberg-Saxton optical correlation,” IEEE Photon. J. **10**, 7800409 (2018).
[30] A. W. Lohmann, “Image rotation, Wigner rotation, and the fractional Fourier transform,” J. Opt. Soc. Am. A **10**, 2181–2186 (1993).

[31] H. M. Ozaktas, Z. Zalevsky, and M. A. Kutay, The Fractional Fourier Transform With Applications in Optics and Signal Processing (Wiley, 2001).
[32] E. Pérez-Cabré, M. Cho, and B. Javidi, "Information authentication using photon-counting double-random-phase encrypted images," Opt. Lett. **36**, 22–24 (2011).
[33] W. Chen, "Single-shot imaging without reference wave using binary intensity pattern for optically-secured-based correlation," IEEE Photon. J. **8**, 6900209 (2016).
[34] W. Chen and X. Chen, "Grayscale object authentication based on ghost imaging using binary signals," EPL **110**, 44002 (2015).
[35] W. Chen and X. Chen, "Marked ghost imaging," Appl. Phys. Lett. **104**, 251109 (2014).
[36] W. Chen, B. Javidi, and X. Chen, "Advances in optical security systems," Adv. Opt. Photon. **6**, 120–155 (2014).
[37] W. Chen and X. Chen, "Object authentication in computational ghost imaging with the realizations less than 5% of Nyquist limit," Opt. Lett. **38**, 546–548 (2013).
[38] X. Wang, W. Chen, S. Mei, and X. Chen, "Optically secured information retrieval using two authenticated phase-only masks," Sci. Rep. **5**, 15668 (2015).
[39] W. Chen, "Multiple-wavelength double random phase encoding with CCD-plane sparse-phase multiplexing for optical information verification," Appl. Opt. **54**, 10711–10716 (2015).
[40] W. Chen, "Virtually optical information verification with a hierarchical structure," Opt. Eng. **57**, 010502 (2018).